Research Paper
Computational Methods for Differential Equations
http://cmde.tabrizu.ac.ir
Vol. *, No. *, *, pp. 1-18
DOI:10.22034/cmde.2026.69521.3427

Enhanced MLS-NN collocation for fractional EHD flows in cylindrical conduits

Parisa Rahimkhani[1,*], **Zahra Khoddami Maraghi**[2,*], **and Ehsan Arshid**[2]
[1]Faculty of Science, Mahallat Institute of Higher Education, Mahallat, Iran.
[2]Faculty of Engineering, Mahallat Institute of Higher Education, Mahallat, Iran.

Abstract

This study presents a hybrid numerical framework that combines the enhanced moving least squares (MLS) approximation, neural networks, and spectral methods to solve a fractional-order electrohydrodynamics flow model in a cylindrical conduit. The proposed method transforms the governing problem into a nonlinear system of algebraic equations. The enhanced MLS technique facilitates the construction of smooth approximations for scattered or irregular data distributions, while the neural network component provides a flexible mechanism for modeling the nonlinear and memory-dependent behavior inherent in fractional-order systems. By embedding MLS-based shape functions as activation mechanisms, the framework effectively captures the solution. Furthermore, a collocation strategy based on the roots of the Legendre polynomials is employed to minimize the residual associated with the underlying fractional operator. This approach improves numerical accuracy and robustness, as verified by the convergence analysis provided in this study. To show the effectiveness of the proposed method, some numerical results are provided.

Keywords. Fractional Electrohydrodynamics flow, Enhanced moving least squares approximation, Neural networks, Spectral method.
1991 Mathematics Subject Classification. 26A33, 33F05, 92B20.

1. Introduction

Electrohydrodynamics (EHD) encompasses the study of the dynamics of ionized or dielectric fluids subjected to externally applied electric fields and influenced by their surrounding environment. This interdisciplinary field has garnered considerable attention owing to its extensive applications across engineering, biomedical technologies, designing the dielectric pump [13], designing the co-planar micro electrode [6], magnetic endoscopy [30], ink jet devices [7], electrospray mass spectrometry and electrospray nanotechnology [39]. Within these systems, the intricate interplay between electric forces and fluid dynamics critically governs the transport phenomena of charged particles through confined geometries.

The conventional mathematical framework describing EHD flow within a cylindrical conduit culminates in a nonlinear singular boundary value problem. This governing model is derived from the fundamental balance between electrical body forces and viscous stresses acting on the fluid medium and is typically represented by a second-order nonlinear ordinary differential equation [9, 18]:

$$Z''(t) + \frac{1}{t}Z'(t) + H^2\left(1 - \frac{Z(t)}{1-\alpha Z(t)}\right) = 0, \tag{1.1}$$

$$Z'(0) = \beta_1, \qquad Z(1) = \beta_2. \tag{1.2}$$

In Eq. (1.1), we have

$$H = \sqrt{\frac{J_0 r^2}{\tau\kappa^2 E_0}}, \qquad \alpha = \frac{\rho_z \kappa}{J_0} - 1.$$

Received: 06 October 2025; Accepted: 28 July 2026.
* Corresponding author. Email: rahimkhani.parisa@mahallat.ac.ir, rahimkhani.parisa@gmail.com, z.khoddami@gmail.com.

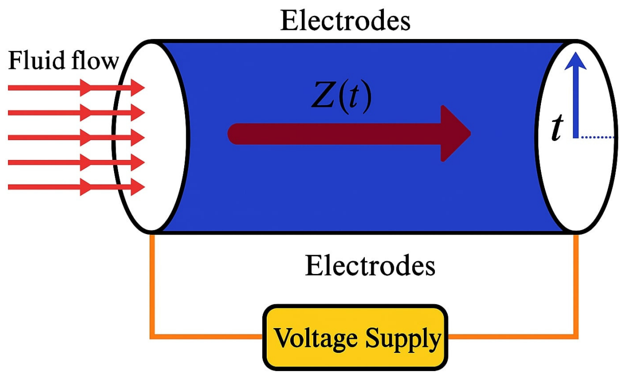

FIGURE 1. Schematic representation of EHD flow in a circular cylindrical conduit.

TABLE 1. Parameters utilized in this study.

Parameter	Description
$Z(t)$	Dimensionless fluid velocity
t	Radial range measured from the center of the conduit
H	Hartmann electric number
J_0	Uniform electrical current density at the inlet
τ	Viscosity of the fluid
κ	Mobility of the ions
ρ_z	Pressure gradient
α	Nonlinearity term
E_0	Electric field
r	Radius of the conduit (before non dimensionalization)

A detailed description of the parameters is provided in Table 1. Also, Figure 1 presents a schematic illustration of the EHD flow within a circular cylindrical conduit.

While several analytical and numerical methods such as iterative algorithm [32], Taylor series method [21], least square method [12], collocation and fourth-order Runge-Kutta method [11], have been proposed to approximate the solution of this classical model, they often fail to accurately capture memory-dependent and hereditary effects.

To overcome this limitation, fractional calculus has emerged as a powerful modeling tool. Fractional differential equations (FDEs) generalize classical models by incorporating non-local derivatives, thereby accounting for the cumulative history of the system. In the context of EHD flow, fractional-order models provide a more realistic representation of the ionized fluid dynamics by considering the influence of past states on the current flow behavior. Motivated by this, the classical EHD model is extended to its fractional-order form using Caputo derivatives. The fractional-order model is given by:

$$ {}^{C}D^{\nu} Z(t) + \frac{1}{t} {}^{C}D^{\zeta} Z(t) + H^2\left(1 - \frac{Z(t)}{1-\alpha Z(t)}\right) = 0, \quad 0 < t < 1, 1 < \nu \leq 2, 0 < \zeta \leq 1. \tag{1.3} $$

$$ Z'(0) = \beta_1, \qquad Z(1) = \beta_2, \tag{1.4} $$

In this model, ${}^{C}D^{\nu}$ is denote the Caputo fractional derivatives of order ν that is defined as [26, 27]:

$$ {}^{C}D^{\nu} Z(t) = \tfrac{1}{\Gamma(n-\nu)} \int_0^t (t-s)^{n-s-1} Z^{(n)}(s) ds, \qquad n-1 < \nu \leq n, $$

where $n \in \mathbb{N}, t > 0$ and $Z \in C^n_{-1}$.
The Riemann–Liouville fractional integral operator of order $\nu \geq 0$ for a function $Z \in C_\varrho, \varrho \geq -1$, is also defined as follows:

$$^{R}I_t^{\nu} Z(t) = \frac{1}{\Gamma(\nu)} \int_0^t (t-s)^{\nu-1} Z(s) ds, \qquad t > 0. \tag{1.5}$$

The inclusion of fractional-order terms significantly enhances the model's capacity to describe complex flow behaviors, including anomalous diffusion and long-memory responses. Due to the lack of closed-form solutions for most fractional models, numerical methods play a vital role in solving such equations [33, 37]. Among these, moving least squares approximation, neural networks and spectral method have shown exceptional accuracy and efficiency, making them ideal for simulating both classical and fractional-order EHD flows.
In recent decades, the MLS method has established itself as a robust and versatile meshless numerical technique, widely acclaimed for its flexibility and computational efficiency in solving a broad class of differential and integral equations. Distinct from conventional mesh-based approaches, the MLS method eliminates the need for discretizing the problem domain into structured grids or finite elements [19, 36]. This attribute renders it particularly well-suited for addressing problems defined over complex geometries, irregular domains, or in high-dimensional settings. The fundamental principle of the MLS method involves constructing smooth approximations of unknown functions by utilizing a set of scattered nodes combined with suitably chosen weight functions defined over localized support domains. This localized formulation enables the generation of relatively small algebraic systems, thereby enhancing computational efficiency while preserving significant flexibility in the distribution of nodes. Furthermore, the independence of the method from a predefined mesh structure allows it to naturally accommodate large deformations, evolving geometries, and topological changes—scenarios that often pose considerable challenges in traditional mesh-dependent techniques due to the associated cost of mesh generation and refinement. Owing to these strengths, the MLS approach has found widespread applications across numerous areas in computational mathematics. It has been effectively employed to solve a diverse range of mathematical models, including third-kind Volterra integral equations with proportional delays [2], fractional integral equations [5], stochastic Volterra integro-differential equation [20] and third-kind auto-convolution Volterra integral equations [3]. A key factor contributing to its widespread adoption is its capacity to deliver accurate approximate solutions using a relatively small number of basis functions and collocation points, which significantly reduces computational overhead without compromising solution quality.
Also, the neural networks (NNs) have gained significant prominence as robust and versatile computational tools for the numerical solution of differential equations. Their universal function approximation capabilities have established them as a powerful alternative to traditional numerical methods, enabling the derivation of analytical and continuous solutions without the necessity for mesh generation or domain discretization. This intrinsic mesh-free characteristic, coupled with the ability of NNs to generalize across complex and irregular domains, renders them particularly effective for addressing a wide spectrum of mathematical and physical problems. The application of NNs spans a diverse array of differential equations, ranging from classical formulations to advanced high-dimensional and nonlinear systems. Notably, NNs have demonstrated exceptional performance in solving canonical problems such as nonlinear stochastic differential equations with fractional Brownian motion [24], heat transfer equation [41], Fokker–Planck equations with low-rank separation representation [40], Burger-Huxley & Huxley's equation [16], fractal-fractional pantograph differential equations [25], stochastic biological systems [23], fuzzy differential equations [8], Thomas-Fermi equation [17] and high-dimensional partial differential equations [14]. Recent advancements have also shown their suitability for solving high-dimensional semi-linear parabolic partial differential equations, highlighting the scalability and adaptability of NNs-based approaches in modern computational mathematics.
The spectral methods also have emerged as accurate and efficient techniques for solving fractional ordinary differential equations (FODEs) ([28, 29]), particularly when dealing with problems characterized by smooth and continuous solutions. By leveraging operational matrices for derivatives and integrals constructed from orthogonal polynomials, these methods facilitate rapid and precise computations across a wide range of problems with varying initial and boundary conditions. Nonetheless, the application of spectral methods to domains featuring irregular boundaries and complex behaviors introduces significant challenges. The necessity to employ multiple operational matrices tailored to specific scenarios—such as boundary conditions, initial conditions, and variable coefficients—often leads to increased

computational overhead and diminished user convenience. Consequently, enhancing and optimizing spectral methods to reduce computational demands and bolster their robustness in handling intricate domains continues to be a central focus of ongoing research in computational mathematics.

In addition to numerical methods developed specifically for fractional differential equations, related advances in other complex dynamical and financial models also provide useful computational perspectives. For example, Ahmadian et al. [1] developed extremely efficient numerical methods for option pricing in the Black-Scholes model with jumps, while Safdari-Vaighani et al. [34] proposed an approximation scheme for option pricing under a two-state continuous CAPM framework. These works demonstrate effective numerical treatments for jump-diffusion and regime-dependent systems, which are relevant from a broader modeling and computational viewpoint. Moreover, the stability analysis presented in [10] for improved backward Euler methods applied to stochastic delay differential equations of neutral type offers an interesting theoretical parallel to the convergence considerations addressed in the present work.

In this study, we propose a novel hybrid approach that synergistically combines the key advantages of three powerful computational methods. By integrating the flexibility and mesh-free nature of the MLS method, the adaptive learning capabilities of NNs, and the spectral methods' high accuracy and computational efficiency, our methodology aims to establish a robust and generalizable framework. This integrated approach is specifically designed to effectively solve the fractional-order EHD flow model within cylindrical conduits, addressing the complex dynamics and nonlocal behaviors inherent in such systems. The proposed method not only enhances solution accuracy but also improves computational efficiency and adaptability to varying problem domains, making it a promising tool for advanced modeling in EHD and related fields.

Accordingly, the main novelties and contributions of the present study can be summarized as follows:

- Introduction of a MLS-NN collocation framework: this study proposes a novel hybrid computational framework that integrates enhanced moving least squares (MLS) approximation, neural networks, and Legendre-based spectral collocation for solving fractional-order electrohydrodynamics flow models. This integration provides a unified mesh-free strategy for handling nonlinear and nonlocal fractional problems.
- Embedding of enhanced MLS shape functions into the neural architecture: unlike conventional neural networks that rely on standard activation functions such as sigmoid or ReLU, the proposed MLSNN employs enhanced MLS-based shape functions as activation mechanisms within the hidden layer. This design improves the approximation capability of the network for complex fractional-order dynamics.
- Novel approximation of the fractional integral operator via Gauss–Legendre numerical integration: in the proposed hybrid MLS-NN collocation framework, the resulting fractional integral operator is approximated using Gauss–Legendre quadrature. This treatment provides an accurate and efficient numerical evaluation of the integral term, improves residual computation, and contributes to the overall stability and robustness of the method.
- Efficient transformation of the governing problem into a nonlinear algebraic system: by applying the properties of the fractional Riemann–Liouville integral operator and a Legendre-root collocation strategy, the original fractional differential model is reduced to a nonlinear system of algebraic equations, which simplifies the numerical implementation and reduces computational complexity.
- Rigorous convergence analysis: the study establishes convergence properties of the proposed MLS-NN approximation in a weighted space, providing a theoretical guarantee for the reliability and stability of the method.

Table 2 provides a comparative analysis of the main characteristics of the proposed MLS-NN collocation method in comparison with pure neural network approaches, traditional numerical methods (such as finite difference (FD) and spectral methods), and pure MLS-based methods. The comparison is presented in terms of computational efficiency, accuracy, flexibility, and implementation challenges. As can be seen, the proposed hybrid framework combines the mesh-free flexibility of MLS approximation, the nonlinear representation capability of neural-network-inspired structures, and the high accuracy of spectral collocation. Therefore, it offers a more balanced and effective approach for solving fractional-order nonlocal problems, particularly in cases involving irregular domains, memory effects, and complex differential operators.

TABLE 2. Comparison of the proposed MLS-NN collocation method with existing approaches.

Comparison Criteria	Pure Neural Network	Traditional Numerical (FD/Spectral)	Pure MLS Methods	Proposed MLS-NN
Computational Efficiency	Reduces reliance on large datasets	Requires fine discretization, high cost	High cost for matrix construction/inversion	High efficiency; mesh-free with fast spectral convergence
Accuracy	Competitive but variable accuracy	Sensitive to mesh quality/refinement	Good for irregular domains; struggles with high-order derivatives	Good accuracy (hybrid MLS + spectral collocation)
Flexibility	High, but difficult to interpret	Limited to regular domains/structures	Very high (mesh-free)	Very high flexibility and mathematical stability
Challenges	Loss function design and weighting	Complex grid generation	Sensitivity to support domain parameters	Precise optimization of hybrid weighting function

The organization of this paper is structured as follows: In Section 2, fundamental definitions and theoretical foundations related to the MLS method and NN techniques are reviewed. Section 3 focuses on the detailed implementation of the proposed hybrid scheme for solving the formulated problem. The convergence analysis of the adopted approach are rigorously examined in Section 4. Section 5 presents and discusses the numerical results that validate the effectiveness of the methodology. Finally, Section 6 concludes the paper with a summary of key findings and potential directions for future research.

2. Fundamentals

2.1. **Enhanced moving least squares method.** In this section, we briefly present the moving least squares approximation method, adhering to the formulations provided in [2, 20].

Definition 2.1 ([2, 38])**.** The MLS approximation, denoted by $S_{Z,N}$, is obtained by solving the following weighted least squares minimization problem for each $t \in O$:

$$\min\{\sum_{i=0}^{n}[Z(t_i) - \mathcal{P}(t_i)]^2\omega_i(t) : \mathcal{P} \in P_q\}, \tag{2.1}$$

where $\omega : O \times O \to \mathbb{R}$, is a continuous weight function, and P_q denotes the space of polynomials of degree less than q.

Definition 2.2 ([2, 38])**.** A set of nodes $N = \{t_0, t_1, \dots, t_n\}$ is said to be q-unisolvent if the only polynomial in that vanishes at all nodes in N is the zero polynomial.

Definition 2.3 ([2, 38])**.** If the set $\{t_0, t_1, \dots, t_n\}$ is q-unisolvent for all $t \in O$, then the minimization problem in (2.1) admits a unique solution, given by:

$$S_{Z,N}(t) = \sum_{i=0}^{n} \phi_i(t) Z(t_i),$$

where the basis functions $\phi_i(t)$ are defined as:

$$\phi_i(t) = \omega_i(t) \sum_{r=0}^{E} g_r f_r(t_i),$$

where coefficients $g_0, g_1, \dots, g_E$ satisfy the linear system:

$$\sum_{r=0}^{E} g_r \sum_{i=0}^{n} \omega_i(t)\mathcal{P}_r(t_i)\mathcal{P}_l(t_i) = \mathcal{P}_l(t), \qquad 0 \le l \le E.$$

To construct the MLS approximation $\hat{Z}(t)$ for $t \in O$, we utilize a set of data points (t_i, Z_i), for $i = 0, 1, \dots, n$. The approximation is expressed as

$$\hat{Z}(t) = f^T(t)a(t), \tag{2.2}$$

where $f(t) = [f_0(t), f_1(t), \dots, f_m(t)]^T$, is the polynomial basis for P_q, and $a(t) = [a_0(t), a_1(t), \dots, a_m(t)]^T$ is the coefficient vector to be determined.

The coefficients are obtained by minimizing the weighted least squares functional:

$$J[\hat{Z}] = \sum_{i=0}^{n} \omega_i(t)(\hat{Z}(t_i) - Z_i)^2. \tag{2.3}$$

Here, $\omega_i : O \times O \to \mathbb{R}$ is the weight corresponding to the node i, and n represents the number of nodes in the domain O for which $\omega_i(t) > 0$. Among various weight functions, we adopt a third-degree spline-type function defined as:

$$\omega(\ell_i) = \begin{cases} \frac{\exp[-(\frac{\ell_i}{\sigma})^2] - \exp[-(\frac{\zeta}{\sigma})^2]}{1-\exp[-(\frac{\zeta}{\sigma})^2]}, & 0 \le \ell_i \le \zeta, \\ 0, & \ell_i > \zeta, \end{cases} \tag{2.4}$$

where $\ell_i = |t - t_i|$, ζ denotes the support size, and σ is the shape parameter that controls the spread of the weight function.
Minimizing J leads to the normal equations:

$$J[\hat{Z}] = \sum_{i=0}^{n} \omega_i(t)(f^T(t_i)a(t) - Z_i)^2. \tag{2.5}$$

To find the extremum of J in Eq. (2.5), we set the derivative of J with respect to the coefficient vector $a(t)$ to zero. This yields the following system of equations:

$$\begin{aligned} &\sum_{i=0}^{n} 2\omega_i(t)f_0(t_i)(f^T(t_i)a(t) - Z_i) = 0, \\ &\sum_{i=0}^{n} 2\omega_i(t)f_1(t_i)(f^T(t_i)a(t) - Z_i) = 0, \\ &\vdots \\ &\sum_{i=0}^{n} 2\omega_i(t)f_m(t_i)(f^T(t_i)a(t) - Z_i) = 0. \end{aligned} \tag{2.6}$$

Reorganizing the terms in Eq. (2.6) leads to the following expression:

$$\sum_{i=0}^{n} 2\omega_i(t)f(t_i)f^T(t_i)a(t) = \sum_{i=0}^{n} 2\omega_i(t)f(t_i)Z_i. \tag{2.7}$$

Define

$$\mathcal{A}(t) = \sum_{i=0}^{n} \omega_i(t)f(t_i)f^T(t_i), \qquad \tilde{Z} = [Z_0, Z_1, \dots Z_n]^T.$$

The moment matrix $\mathcal{A}(t)$, which is of size $(m+1) \times (m+1)$, is defined as follows:

$$\mathcal{H}(t) = [\omega_0(t)f(t_0), \omega_1(t)f(t_1), \dots, \omega_n(t)f(t_n)].$$

As a result, we derive

$$\mathcal{A}(t)a(t) = \mathcal{H}(t)\tilde{Z}. \tag{2.8}$$

The node points are selected to ensure that the matrix $\mathcal{A}(t)$ remains nonsingular. Under this condition, Eq. (2.8) can be reformulated as:

$$a(t) = \mathcal{A}^{-1}(t)\mathcal{H}(t)\tilde{Z}. \tag{2.9}$$

Substituting Eq. (2.9) into Eq. (2.2) leads to the following expression:

$$\hat{Z}(t) = f^T(t)\mathcal{A}^{-1}(t)\mathcal{H}(t)\tilde{Z} = \sum_{i=0}^{n} \phi_i(t)Z_i, \qquad t \in O, \tag{2.10}$$

where

$$\phi_i(t) = \sum_{r=0}^{m} f_r(t)[\mathcal{A}^{-1}(t)\mathcal{H}(t)]_{ri}. \tag{2.11}$$

The shape functions $\phi_i(t)$ in the MLS approximation are associated with the corresponding nodal points t_i. If $\omega_i(t) \in C^{v_1}(O)$ and $f_r(t) \in C^{v_2}(O)$ for $i = 0, 1, \dots, n; r = 0, 1, \dots, m$, then $\phi_i(t) \in C^{min(v_1,v_2)}(O)$.
In general, various types of basis functions can be employed within the proposed method. In this study, the fractional-order airfoil functions are employed as the basis functions. The fractional-order airfoil functions on the interval $[0, 1]$ are defined as:

$$Airfoil_j^\lambda(t) = \sum_{\ell=0}^{j} \sum_{i=j-\ell}^{\ell} (-1)^{2i-j+\ell} \left(\begin{array}{c} 2j+1 \\ 2i+1 \end{array} \right) \left(\begin{array}{c} i \\ j-\ell \end{array} \right) t^{\lambda\ell}, \quad 0 < \lambda \leq 1. \tag{2.12}$$

The fractional-order airfoil functions are governed by the following relationship:

$$\int_0^1 Airfoil_i^\lambda(t) Airfoil_j^\lambda(t) \mathcal{W}^\lambda(t) t^{\lambda-1} dt = \frac{\pi}{2\lambda}\delta_{ij}, \tag{2.13}$$

where $\mathcal{W}^\lambda(t) = \sqrt{\frac{1-t^\lambda}{t^\lambda}}, t \in (0, 1)$.

2.2. **Neural network method.** In this study, we employ a NN-based framework, termed the enhanced MLS neural network (MLS-NN), to approximate the solutions of the fractional-order EHD flow model in a cylindrical conduit. The enhanced MLS-NN integrates the approximation capabilities of NNs with the properties of enhanced MLS, enhancing both learning efficiency and solution accuracy.

Network Architecture. The enhanced MLS-NN consists of three primary layers:

- Input Layer: This layer consists of a single neuron responsible for receiving the input variable t, which assumes ι discrete values drawn from the dataset $\{t_1, t_2, \dots, t_\iota\}$.
- Hidden Layer: Unlike conventional NNs that commonly use activation functions such as sigmoid or ReLU, the proposed method employs the enhanced MLS approximation as activation functions. This choice enhances the representational capacity of the network and leads to improved numerical accuracy in capturing the intricate solution dynamics of fractional-order systems.
- Output Layer: The outputs generated by the hidden layer-constructed using the enhanced MLS approximation-are linearly aggregated and subsequently processed by a final activation function to yield the network output. Specifically, the output $Network(t, C)$ is expressed as:

  $$Network(t, C) = Activation(\Xi(t, C)), \tag{2.14}$$

  where $Activation(.)$ is the chosen output activation function, and Ξ is a linear combination of the enhanced MLS approximation components as:

  $$\Xi(t, C) = \textstyle\sum_{i=0}^{n} c_i\phi_i(t),$$

  and the vector C is structured as:

  $$C = [c_0, c_1, \dots, c_n]^T.$$

Training Dataset. The training data play a critical role in the performance of the enhanced MLS-NN. Several sampling strategies can be employed, such as equidistant points or roots of orthogonal polynomials. In this work, we construct the training dataset using the roots of the Legendre polynomial, as they provide an efficient and numerically stable distribution of points in the input domain.

Advantages. The proposed enhanced MLS-NN method combines the strengths of the enhanced MLS approximation with the adaptability of NNs. The enhanced MLS technique provides smooth, accurate approximations and is well-suited for handling irregular or scattered data distributions. This makes it particularly advantageous for simulating the complex behavior of fractional-order systems. In addition, the NN component enhances the model's ability to capture nonlinear and memory-dependent features, leading to improved generalization and predictive performance.

Remark 2.4. It is worth noting that the proposed MLS-NN is framed as a neural-network-inspired approximation framework rather than a conventional data-driven learning model. While its architecture resembles deep learning layouts, the training process is governed by the principles of deterministic numerical analysis. In this context, the unknown coefficients of the network play the role of 'trainable parameters', which are determined by minimizing the residual of the governing equation at specific collocation points—acting as the 'loss function'—rather than through backpropagation or stochastic optimization. By integrating the Moving Least Squares method, this framework extends traditional polynomial-based neural network models, providing improved flexibility and convergence properties for solving differential equations.

3. The devised methodology

In this section, a novel hybrid method that combines the enhanced MLS approach with NNs is employed to solve the fractional-order EHD flow model. To this end, the fractional integral operator is constructed for the introduced approximate function.

Lemma 3.1. *The fractional integral operator* $(\Lambda(t,\nu))$ *in the Riemann–Liouville sense of* $Network(t,C)$, *as defined in Eq. (2.14), is derived as follows:*

$$ {}^{R}I^{\nu}(Network(t,C)) = \Lambda(t,\nu), \tag{3.1}$$

where

$$\Lambda(t,\nu) = \tfrac{t}{2\Gamma(\nu)} \textstyle\sum_{j=1}^{n^*} \omega_j (t-(\tfrac{t}{2}(1+\eta_j)))^{\nu-1} Network(\tfrac{t}{2}(1+\eta_j),C).$$

Proof. By applying the Riemann–Liouville fractional integral in Eq. (1.5) and the Legendre-Gauss numerical integration rule [15], we obtain:

$$\begin{aligned} {}^{R}I^{\nu}(Network(t,C)) &= \frac{1}{\Gamma(\nu)}\int_0^t (t-s)^{\nu-1} Network(s,C)ds \\ &= \frac{t}{2\Gamma(\nu)}\int_{-1}^{1} (t-(\frac{t}{2}(1+s)))^{\nu-1} Network(\frac{t}{2}(1+s),C)ds \\ &= \frac{t}{2\Gamma(\nu)}\sum_{j=1}^{n^*} \omega_j (t-(\frac{t}{2}(1+\eta_j)))^{\nu-1} Network(\frac{t}{2}(1+\eta_j),C), \end{aligned} \tag{3.2}$$

where $\{\omega_j\}_{j=1}^{n^*}$ and $\{\eta_j\}_{j=1}^{n^*}$ are the Legendre-Gauss quadrature nodes and weights, respectively. □

Now, we apply the obtained integral operator in Lemma 1 and a novel hybrid method for solving the following the fractional-order EHD flow model:

$$ {}^{C}D^{\nu}Z(t) + \frac{1}{t}{}^{C}D^{\zeta}Z(t) + H^2(1-\frac{Z(t)}{1-\alpha Z(t)}) = 0, \tag{3.3}$$

$$ Z'(0) = \beta_1, \qquad Z(1) = \beta_2, \tag{3.4}$$

where $0 < t < 1, 1 < \nu \leq 2, 0 < \zeta \leq 1$.
First, the highest-order derivative ${}^{C}D^{\nu}Z(t)$ is approximated using the enhanced MLS-NN as follows:

$$ {}^{C}D^{\nu}Z(t) = Network(t,C) = {}^{C}D^{\nu}\hat{Z}(t). \tag{3.5}$$

By taking the Riemann-Liouville fractional integral of order ν to Eq. (3.5), the following relation is obtained:

$$ Z(t) = {}^{R}I^{\nu}(Network(t,C)) + Z(0) + tZ'(0). \tag{3.6}$$

From the fractional integral operator in Eq. (3.1) and the initial condition, we get:

$$ Z(t) = \Lambda(t,\nu) + Z(0) + t\beta_1. \tag{3.7}$$

By setting $t = 1$ in Eq. (3.7), we get

$$ Z(0) = \beta_2 - \Lambda(1,\nu) - \beta_1. \tag{3.8}$$

In the following, based on Eqs. (3.7)-(3.8), an approximation for the unknown function $Z(t)$ is taken as:

$$Z(t) = \Lambda(t,\nu) - \Lambda(1,\nu) + \beta_1 t + (\beta_2 - \beta_1) = \hat{Z}(t). \tag{3.9}$$

To compute the function ${}^{C}D^{\zeta}Z(t)$, we take the fractional derivative of order $0 < \zeta \leq 1$ from Eq. (3.9), thus we get

$${}^{C}D^{\zeta}Z(t) = \Lambda(t,\nu-\zeta) - \Lambda(1,\nu-\zeta) + \frac{\beta_1}{\Gamma(2-\zeta)}t^{1-\zeta} = {}^{C}D^{\zeta}\hat{Z}(t). \tag{3.10}$$

Next, the residual function is constructed as follows:

$$Residual(t) = (1-\alpha\hat{Z}(t))({}^{C}D^{\nu}\hat{Z}(t) + \frac{1}{t}{}^{C}D^{\zeta}\hat{Z}(t) + H^2(1-(\alpha+1)\hat{Z}(t))). \tag{3.11}$$

Consequently, by substituting Eqs. (3.5), (3.9) and (3.10) in Eq. (3.11), the result is:

$$\begin{aligned} Residual(t,C) = {} & (1-\alpha(\Lambda(t,\nu) - \Lambda(1,\nu) + \beta_1 t + (\beta_2-\beta_1)))(Network(t,C) \\ & + \frac{1}{t}(\Lambda(t,\nu-\zeta) - \Lambda(1,\nu-\zeta) + \frac{\beta_1}{\Gamma(2-\zeta)}t^{1-\zeta}) \\ & + H^2(1-(\alpha+1)(\Lambda(t,\nu) - \Lambda(1,\nu) + \beta_1 t + (\beta_2-\beta_1)))). \end{aligned} \tag{3.12}$$

Eq. (3.12) is collocated at the zeros of the Legendre polynomial $(P_{m+1}(t))$ as follows:

$$Residual(t_i, C) = 0, \qquad i = 0, 1, \ldots, m. \tag{3.13}$$

The aforementioned system is solved using Mathematica software packages. Once C is computed, the numerical solution is obtained via Eq. (3.9).

4. Convergence analysis

Here, we establish the convergence of the proposed numerical method for solving the fractional-order EHD flow model presented in the governing Equations (1.3)-(1.4). To this end, we define:

$$< u, v >_t = \sum_{i=1}^{n} \omega_i(t) u(t_i) v(t_i),$$

and observe that

$$\|u\|_t = (< u, u >_t)^{\frac{1}{2}}.$$

Property 4.1 ([42])**.** For every $t \in O$, the matrix $\mathcal{A}(t)$, as defined in Eq. (2.8), is guaranteed to be nonsingular.

Definition 4.2. Given $t \in O$, the set $ST(t) = \{i : \omega_i(t) \neq 0\}$ is referred to as the star of t.

Theorem 4.3 ([4])**.** *A necessary condition for Property 4.1 to hold is that it must be satisfied for every $t \in O$*

$$n = card(ST(t)) \geq card(P_q) = m + 1.$$

Theorem 4.4 ([4])**.** *Let $\mathcal{A}(t)$ satisfies Property 1. Then, for every $t \in O$, there exists $\hat{Z}(t) \in P_q$, such that the following condition holds:*

$$\|Z - \hat{Z}\|_t \leq \|Z - \mathcal{P}\|_t,$$

for all $\mathcal{P} \in P_q$.

Lemma 4.5. *In finite-dimensional vector spaces, norms are equivalent.*

Theorem 4.6 ([35])**.** *Let $Z \in L^2([0,1]) \cap C^{(2)}([0,1])$, and*

$$P_m Z(t) = \sum_{i=0}^{m} c_i Airfoil_i^{\lambda}(t),$$

be the truncated fractional-order airfoil functions series of $Z(t)$. Then, the global error measured in the $L^2([0,1])$ norm satisfies the following estimate:

$$\|Z - P_m Z\|_{L^2([0,1])} \leq \varsigma m^{-\frac{7}{2}},$$

where

$$\varsigma = \sqrt{\tfrac{8}{7\pi}} \max_{t\in[0,1]} |Z''(t)|.$$

Corollary 4.7. *By considering Theorems 4.4 and 4.6 and Lemma 4.5, we conclude*
$$\lim_{m\to\infty} \|Z-\hat{Z}\|_{L^2([0,1])}=0.$$

Lemma 4.8. *Let $Z\in L^2([0,1])\cap C^{(2)}([0,1])$, then we have*
$$\|{}^CD^\nu Z-{}^CD^\nu \hat{Z}\|_{L^2([0,1])}\leq \theta_1\|Z-\hat{Z}\|_{L^2([0,1])}, \qquad 1<\nu\leq 2,$$
and
$$\|{}^CD^\zeta Z-{}^CD^\zeta \hat{Z}\|_{L^2([0,1])}\leq \theta_2\|Z-\hat{Z}\|_{L^2([0,1])}, \qquad 0<\zeta\leq 1.$$

Proof. The proof follows a similar line of reasoning as that presented in Theorem 5.3 of Ref. [22] and Lemma 2 of Ref. [31]. □

Corollary 4.9. *From Corollary 4.7 and Theorem 4.10, we obtain*
$$\lim_{m\to\infty} \|{}^CD^\nu Z-{}^CD^\nu \hat{Z}\|_{L^2([0,1])}=0,$$
and
$$\lim_{m\to\infty} \|{}^CD^\zeta Z-{}^CD^\zeta \hat{Z}\|_{L^2([0,1])}=0.$$

Theorem 4.10. *Suppose that the hypotheses of Theorems 4.3–4.6 are satisfied. Then we have*
$$\lim_{m\to\infty} \|Residual(.,C)\|_{L^2([0,1])}=0.$$

Proof. Utilizing Eqs. (3.3) and (3.11), we get
$$\begin{aligned}
Residual(t,C) &= {}^CD^\nu Z(t)+\frac{1}{t}{}^CD^\zeta Z(t)+H^2-H^2(\alpha+1)Z(t)\\
&-\alpha Z(t){}^CD^\nu Z(t)-\frac{1}{t}\alpha Z(t){}^CD^\zeta Z(t)-H^2\alpha Z(t)+H^2\alpha(\alpha+1)Z^2(t)\\
&-{}^CD^\nu \hat{Z}(t)-\frac{1}{t}{}^CD^\zeta \hat{Z}(t)-H^2+H^2(\alpha+1)\hat{Z}(t)\\
&+\alpha\hat{Z}(t){}^CD^\nu \hat{Z}(t)+\frac{1}{t}\alpha\hat{Z}(t){}^CD^\zeta \hat{Z}(t)+H^2\alpha\hat{Z}(t)-H^2\alpha(\alpha+1)\hat{Z}^2(t).
\end{aligned} \tag{4.1}$$

Now, we can write
$$\begin{aligned}
\|Residual(.,C)\|_{L^2([0,1])} &\leq \|{}^CD^\nu Z-{}^CD^\nu\hat{Z}\|_{L^2([0,1])}+M\|{}^CD^\zeta Z-{}^CD^\zeta\hat{Z}\|_{L^2([0,1])}\\
&+H^2(\alpha+1)\|Z-\hat{Z}\|_{L^2([0,1])}+\alpha\|Z^CD^\nu Z-Z^CD^\nu\hat{Z}\\
&+Z^CD^\nu\hat{Z}-\hat{Z}^CD^\nu\hat{Z}\|_{L^2([0,1])}+M\alpha\|Z^CD^\zeta Z-Z^CD^\zeta\hat{Z}\\
&+Z^CD^\zeta\hat{Z}-\hat{Z}^CD^\zeta\hat{Z}\|_{L^2([0,1])}+H^2\alpha\|Z-\hat{Z}\|_{L^2([0,1])}\\
&+H^2\alpha(\alpha+1)\|Z^2-\hat{Z}^2\|_{L^2([0,1])}\\
&\leq \|{}^CD^\nu Z-{}^CD^\nu\hat{Z}\|_{L^2([0,1])}+M\|{}^CD^\zeta Z-{}^CD^\zeta\hat{Z}\|_{L^2([0,1])}\\
&+H^2(\alpha+1)\|Z-\hat{Z}\|_{L^2([0,1])}+\alpha\|Z\|_{L^2([0,1])}\|D^\nu Z-D^\nu\hat{Z}\|_{L^2([0,1])}\\
&+\alpha\|D^\nu\hat{Z}\|_{L^2([0,1])}\|Z-\hat{Z}\|_{L^2([0,1])}+M\alpha\|Z\|_{L^2([0,1])}\|D^\zeta Z-D^\zeta\hat{Z}\|_{L^2([0,1])}\\
&+M\alpha\|D^\zeta\hat{Z}\|_{L^2([0,1])}\|Z-\hat{Z}\|_{L^2([0,1])}+H^2\alpha\|Z-\hat{Z}\|_{L^2([0,1])}\\
&+H^2\alpha(\alpha+1)\|Z+\hat{Z}\|_{L^2([0,1])}\|Z-\hat{Z}\|_{L^2([0,1])}.
\end{aligned} \tag{4.2}$$

Eq. (4.2) can be reformulated as follows:

$$\begin{aligned}
\|Residual(.,C)\|_{L^2([0,1])} &\leq (1+\alpha N_1)\|{}^CD^\nu Z-{}^CD^\nu\hat{Z}\|_{L^2([0,1])}\\
&+M(1+\alpha N_1)\|{}^CD^\zeta Z-{}^CD^\zeta\hat{Z}\|_{L^2([0,1])}\\
&++(H^2(\alpha+1)(1+\alpha N_3)+\alpha(N_2+N_2'M+H^2))\|Z-\hat{Z}\|_{L^2([0,1])},
\end{aligned} \tag{4.3}$$

where

$$N_1 = \|Z\|_{L^2([0,1])}, \;\; N_2 = \|{}^C D^{\nu} \hat{Z}\|_{L^2([0,1])}, \;\; N_2' = \|{}^C D^{\zeta} \hat{Z}\|_{L^2([0,1])}, \;\; N_3 = \|Z + \hat{Z}\|_{L^2([0,1])}.$$

From Corollaries 4.7 and 4.9, we conclude

$$\lim_{m\to\infty} \|Residual(.,C)\|_{L^2([0,1])} = 0.$$

□

Remark 4.11. Although the present convergence analysis is developed for the proposed fractional numerical framework, it is conceptually consistent with the stability perspective studied by Farkhondeh Rouz and Ahmadian [10] for stochastic delay equations. In particular, their analysis emphasizes the importance of preserving the qualitative dynamical behavior of delayed stochastic systems, while our convergence result ensures that the proposed approximation remains bounded and approaches the exact solution under the stated assumptions. Therefore, the current analysis may be viewed as complementary to that line of stability-oriented research.

5. Simulation Outcomes

In this section, we apply the proposed numerical scheme for various values of n to obtain approximate solutions to the initial value problem (3.3)-(3.4), considering both classical (non-fractional) and fractional-order derivatives. All computations carried out on a personal laptop (Asus creator Laptop Q OLED) equipped with a 2.40 GHz Intel Core i7 processor and 16 GB of RAM. For the classical derivative case, consistent with the existing literature, the parameters were set as $\nu = 2$, and $\zeta = 1$. In contrast, for the fractional-order derivatives, multiple combinations of ν and ζ were considered to examine the behavior of the solution under different fractional dynamics. Given the significance of the nonlinearity parameter α and the Hartmann number H^2 in EHD flows, we systematically analyzed their influence on the solution to Equation (3.3) by varying their values. In our analysis, we let $\sigma = \frac{0.5}{\sqrt{n-1}}$, and $\zeta = \frac{2}{\sqrt{n-1}}$ for the linear case and $\zeta = \frac{2.5}{\sqrt{n-1}}$ for the quadratic case. Since the exact analytical solution to boundary value problem (3.3) is not available, we introduce a residual error (RE) metric as a quantitative measure of how accurately the approximate solution satisfies the governing equation as

$$ResidualError(t) = |(1 - \alpha\hat{Z}(t))({}^C D^{\nu}\hat{Z}(t) + \tfrac{1}{t}{}^C D^{\zeta}\hat{Z}(t) + H^2(1 - (\alpha+1)\hat{Z}(t)))|,$$

where $\hat{Z}(t)$ is the obtained approximated solution by the proposed method.

Table 3 demonstrates the numerical results (NRs) and REs with $H^2 = \alpha = 1, \lambda = \frac{2}{50}, Activation(t) = \sinh(t)$ and $n = 5, 7, 9$ for the non fractional EHD fluid ($\nu = 2, \zeta = 1$). Also, Tables 4-5 report the NRs and REs with $Activation(t) = \sinh(t)$ and different values of n for the fractional EHD fluid ($\nu = 1.9, \zeta = 0.9$ and $\nu = 1.8, \zeta = 0.8$). As shown in Tables 3-5, the accuracy of the method improves significantly as the number of base elements increases. The NRs and REs with $\nu = 1.9, \zeta = 0.9, H^2 = 2, \alpha = 1, n = 9$, $Activation(t) = \sinh(t)$ for $\lambda = \frac{2}{45}, \frac{2}{35}, \frac{2}{31}, \frac{2}{25}, \frac{1}{2}, 1$ have been tabulated in Table 6. Table 6 shows the effect of the parameter λ for this problem. Table 7 presents the NRs and REs with $\nu = 1.95, \zeta = 0.95, H^2 = 2, \alpha = 0.5, n = 11, \lambda = \frac{2}{50}$ for $Activation(t) = t$ and $Activation(t) = \sinh(t)$. In this Table, the computational efficiency of the proposed scheme is highlighted through $Activation(t)$ metrics. Figures 2-5 present the obtained numerical solutions corresponding to $\nu = 1.9, \zeta = 0.9$, $Activation(t) = \sinh(t)$ and from a physical standpoint, it is well-understood that the fluid velocity tends to increase as either the viscosity or the applied electric field within the fluid decreases. Since the nonlinear parameter α is independent of these terms, the most straightforward approach to modifying the Hartmann number without altering the nonlinearity is by adjusting the electric field E_0 or the fluid viscosity τ. A reduction in these parameters, while keeping α constant, results in an increase in the Hartmann number. This physical behavior-namely, that an increase in the Hartmann number for a fixed nonlinearity leads to a higher fluid velocity-is clearly reproduced in these figures. In fact, Figures 2 and 3 specifically highlight the effect of the parameter $\lambda\,(\lambda = \frac{2}{50}, 1)$ in this example. The significance of the obtained numerical solution for $\nu = 1.9, \zeta = 0.9, \lambda = \frac{2}{50}, n = 9$, $Activation(t) = \sinh(t)$ under varying values of the nonlinearity parameter α, with a fixed Hartmann number H^2, is illustrated in Figure 6. The figure captures the physical behavior whereby the fluid velocity $Z(t)$ decreases as the nonlinearity parameter α increases, for constant values of H^2. In other words, as the degree of nonlinearity shifts from weak to strong, a corresponding reduction in $Z(t)$ is observed. Furthermore,

Figure 6 graphically demonstrates that, with increasing α, the velocity profiles tend to converge more closely for lower values of H^2, in contrast to the more dispersed behavior observed for higher values of H^2. The influence of fractional differentiation on the solution behavior, with constant α and H^2 and varying ν and ζ, is demonstrated in Figures 7 and 8 for $n = 9, \lambda = \frac{2}{50}$, $Activation(t) = \sinh(t)$.

TABLE 3. The NRs and REs with $\nu = 2, \zeta = 1, H^2 = \alpha = 1, \lambda = \frac{2}{50}$ and $Activation(t) = \sinh(t)$.

t	$n = 5$		$n = 7$		$n = 9$	
	NRs	REs	NRs	REs	NRs	REs
0.1	0.800442	2.36×10^{-2}	1.036780	8.25×10^{-2}	0.837975	7.69×10^{-4}
0.2	0.712817	6.14×10^{-3}	0.911183	6.38×10^{-2}	0.746146	1.33×10^{-4}
0.3	0.628019	9.34×10^{-3}	0.790277	2.38×10^{-3}	0.657445	6.27×10^{-4}
0.4	0.544793	9.44×10^{-3}	0.676349	3.91×10^{-2}	0.570121	9.29×10^{-4}
0.5	0.461670	1.44×10^{-13}	0.567084	4.35×10^{-14}	0.482784	2.03×10^{-13}
0.6	0.377182	7.57×10^{-3}	0.459022	2.43×10^{-2}	0.394111	8.35×10^{-4}
0.7	0.289989	6.05×10^{-3}	0.349806	9.72×10^{-4}	0.302813	5.05×10^{-4}
0.8	0.198884	3.17×10^{-3}	0.238009	1.94×10^{-2}	0.207608	9.45×10^{-5}
0.9	0.102673	7.92×10^{-3}	0.122085	1.38×10^{-2}	0.107146	2.91×10^{-4}

TABLE 4. The NRs and REs with $\nu = 1.9, \zeta = 0.9, H^2 = 2, \alpha = 0.5, \lambda = \frac{2}{50}$ and $Activation(t) = \sinh(t)$.

t	$n = 5$		$n = 7$		$n = 9$	
	NRs	REs	NRs	REs	NRs	REs
0.1	1.099780	1.27×10^{-3}	1.150970	7.29×10^{-3}	1.185670	7.71×10^{-4}
0.2	0.972906	2.27×10^{-3}	1.016270	6.15×10^{-3}	1.045100	1.29×10^{-4}
0.3	0.857350	5.20×10^{-3}	0.893847	2.18×10^{-4}	0.917869	5.68×10^{-4}
0.4	0.746946	6.36×10^{-3}	0.777244	3.97×10^{-3}	0.797069	4.12×10^{-4}
0.5	0.637666	4.01×10^{-13}	0.662297	1.06×10^{-13}	0.678297	2.96×10^{-13}
0.6	0.526186	6.16×10^{-3}	0.545559	3.69×10^{-3}	0.558066	5.48×10^{-4}
0.7	0.409532	5.09×10^{-3}	0.423950	1.64×10^{-4}	0.433227	4.14×10^{-4}
0.8	0.284902	2.64×10^{-3}	0.294559	2.96×10^{-3}	0.300732	6.27×10^{-5}
0.9	0.149449	6.26×10^{-3}	0.154352	1.71×10^{-3}	0.157439	1.24×10^{-4}

TABLE 5. The NRs and REs with $\nu = 1.8, \zeta = 0.8, H^2 = 0.5, \alpha = 1, \lambda = \frac{2}{31}$ and $Activation(t) = \sinh(t)$.

t	$n = 6$		$n = 8$		$n = 10$	
	NRs	REs	NRs	REs	NRs	REs
0.1	0.657258	4.69×10^{-2}	0.660553	9.40×10^{-4}	0.667848	9.80×10^{-3}
0.2	0.567034	1.14×10^{-2}	0.571233	7.65×10^{-3}	0.577989	5.63×10^{-3}
0.3	0.488734	1.42×10^{-2}	0.493023	7.90×10^{-3}	0.498878	2.03×10^{-3}
0.4	0.416413	3.01×10^{-3}	0.420094	9.40×10^{-4}	0.425311	2.31×10^{-3}
0.5	0.346946	8.95×10^{-3}	0.350114	4.62×10^{-3}	0.354638	3.09×10^{-3}
0.6	0.278713	1.80×10^{-3}	0.281537	4.14×10^{-4}	0.285175	9.45×10^{-4}
0.7	0.210754	5.42×10^{-3}	0.213082	1.77×10^{-3}	0.215853	4.61×10^{-4}
0.8	0.142229	2.86×10^{-3}	0.143831	1.07×10^{-3}	0.145731	8.98×10^{-4}
0.9	0.072243	6.05×10^{-3}	0.073049	6.91×10^{-5}	0.074012	8.35×10^{-4}

Table 6. The NRs and REs with $\nu = 1.9, \zeta = 0.9, H^2 = 2, \alpha = 1, n = 9$ and $Activation(t) = \sinh(t)$.

t	$\lambda = \frac{2}{45}$	$\lambda = \frac{2}{35}$	$\lambda = \frac{2}{31}$	$\lambda = \frac{2}{25}$	$\lambda = \frac{1}{2}$	$\lambda = 1$
0.1	3.59×10^{-2}	1.22×10^{-4}	6.27×10^{-5}	1.40×10^{-5}	1.60×10^{-2}	7.06×10^{-2}
0.2	6.12×10^{-3}	1.13×10^{-4}	5.39×10^{-5}	8.54×10^{-5}	3.82×10^{-2}	5.65×10^{-3}
0.3	2.09×10^{-2}	4.52×10^{-4}	8.26×10^{-4}	7.52×10^{-4}	1.22×10^{-1}	3.81×10^{-4}
0.4	2.30×10^{-2}	3.29×10^{-4}	2.00×10^{-4}	1.37×10^{-3}	1.21×10^{-1}	1.15×10^{-2}
0.5	1.27×10^{-13}	5.33×10^{-14}	9.25×10^{-14}	2.11×10^{-14}	6.32×10^{-14}	2.56×10^{-14}
0.6	1.25×10^{-2}	3.64×10^{-4}	6.83×10^{-4}	1.38×10^{-3}	8.48×10^{-2}	2.26×10^{-2}
0.7	7.24×10^{-3}	2.91×10^{-4}	4.78×10^{-4}	8.90×10^{-4}	6.04×10^{-2}	2.30×10^{-2}
0.8	1.61×10^{-3}	4.64×10^{-5}	9.02×10^{-5}	1.87×10^{-4}	1.53×10^{-1}	6.83×10^{-3}
0.9	6.14×10^{-3}	9.73×10^{-5}	2.73×10^{-4}	6.62×10^{-4}	5.88×10^{-2}	2.96×10^{-2}

Table 7. The NRs and REs with $\nu = 1.95, \zeta = 0.95, H^2 = 2, \alpha = 0.5, n = 11, \lambda = \frac{2}{50}$.

t	$Activation(t) = t$		$Activation(t) = \sinh(t)$	
	NRs	REs	NRs	REs
0.1	1.568750	6.91×10^{-1}	1.194480	4.76×10^{-3}
0.2	1.368620	5.22×10^{-1}	1.058380	1.40×10^{-3}
0.3	1.779200	5.74×10^{-1}	0.931970	8.81×10^{-4}
0.4	1.008990	3.78×10^{-1}	0.810271	3.78×10^{-4}
0.5	0.842093	7.07×10^{-11}	0.689718	1.83×10^{-13}
0.6	0.678795	1.47×10^{-1}	0.567263	4.64×10^{-5}
0.7	0.517808	1.22×10^{-1}	0.440028	4.55×10^{-5}
0.8	0.352483	8.69×10^{-2}	0.305123	6.20×10^{-5}
0.9	0.181100	7.56×10^{-2}	0.159531	7.76×10^{-5}

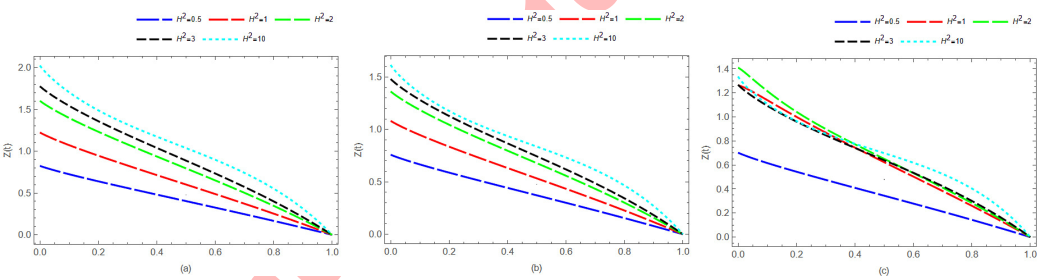

Figure 2. Diagrams of $Z(t)$ for $(a) : \alpha = 0.2; (b) : \alpha = 0.5; (c) : \alpha = 0.8$ with $\nu = 1.9, \zeta = 0.9, \lambda = \frac{2}{50}, n = 9$ and $Activation(t) = \sinh(t)$.

6. Conclusion

The proposed hybrid numerical framework-integrating the enhanced MLS approximation, NNs, and spectral collocation methods-has been effectively employed to solve a fractional-order EHD flow model within a cylindrical conduit. The numerical experiments confirm the framework's ability to deliver accurate results with strong convergence behavior and numerical stability. These outcomes underscore the method's robustness in capturing the complex, nonlocal, and memory-dependent dynamics intrinsic to fractional-order systems. A key innovation lies in the incorporation of enhanced MLS-derived shape functions as activation mechanisms within the NN architecture, which substantially improves approximation accuracy while enhancing computational efficiency. Additionally, the adoption of a collocation scheme based on the Legendre polynomial roots significantly contributes to the stability and precision of the numerical scheme, particularly in addressing the nonlinear characteristics of the governing equations. Furthermore, the established convergence of the proposed method substantiates its theoretical robustness and affirms the reliability

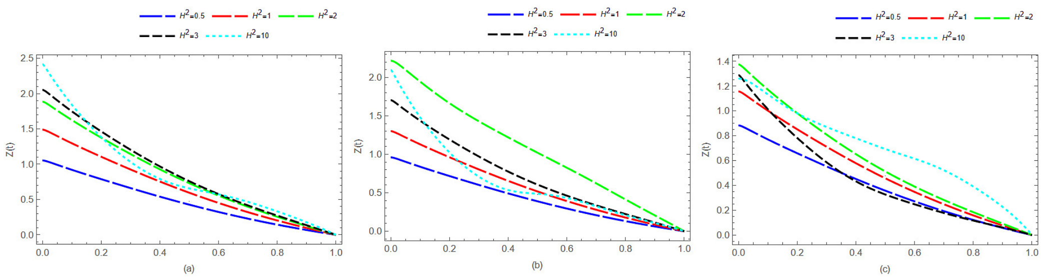

FIGURE 3. Diagrams of $Z(t)$ for $(a): \alpha = 0.2; (b): \alpha = 0.5; (c): \alpha = 0.8$ with $\nu = 1.9, \zeta = 0.9, \lambda = 1, n = 9$ and $Activation(t) = \sinh(t)$.

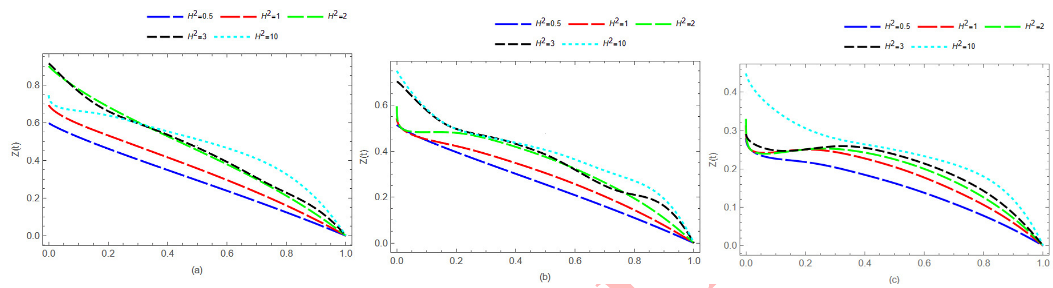

FIGURE 4. Diagrams of $Z(t)$ for $(a): \alpha = 1.5; (b): \alpha = 2; (c): \alpha = 4$ with $\nu = 1.9, \zeta = 0.9, \lambda = \frac{2}{50}, n = 9$ and $Activation(t) = \sinh(t)$.

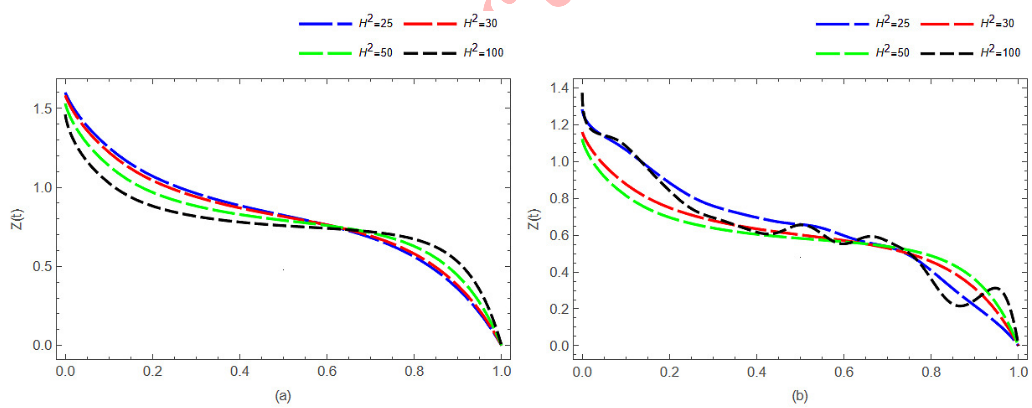

FIGURE 5. Diagrams of $Z(t)$ for $(a): \alpha = 0.5; (b): \alpha = 1$; with $\nu = 1.9, \zeta = 0.9, \lambda = \frac{2}{31}, n = 11$ and $Activation(t) = \sinh(t)$.

of its numerical performance, even in the absence of exact analytical solutions. Looking ahead, the proposed framework offers promising avenues for extension and application. Potential future directions include its generalization to higher-dimensional fractional models, integration into fractional optimal control and inverse problems, and coupling with advanced machine learning paradigms such as convolutional NNs or reinforcement learning, thereby broadening its applicability to more complex and computationally intensive real-world scenarios. Also, future research will focus on the following directions:

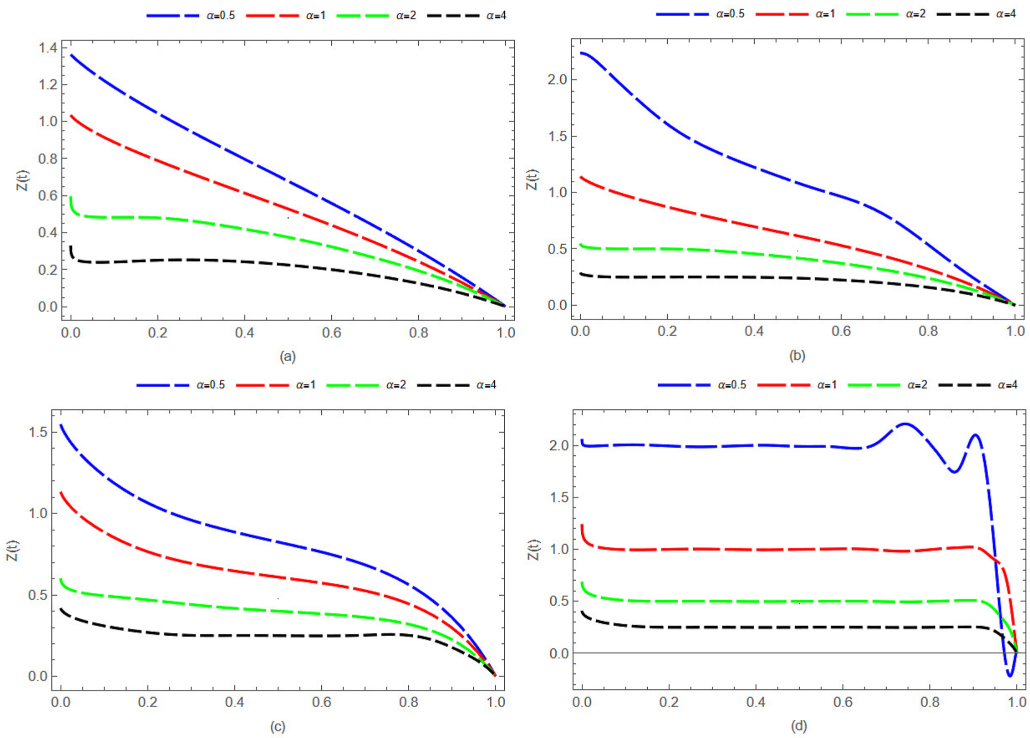

FIGURE 6. Diagrams of $Z(t)$ for $(a): H^2 = 2; (b): H^2 = 5; (c): H^2 = 25; (d): H^2 = 100$; with $\nu = 1.9, \zeta = 0.9, \lambda = \frac{2}{50}, n = 9$ and $Activation(t) = \sinh(t)$.

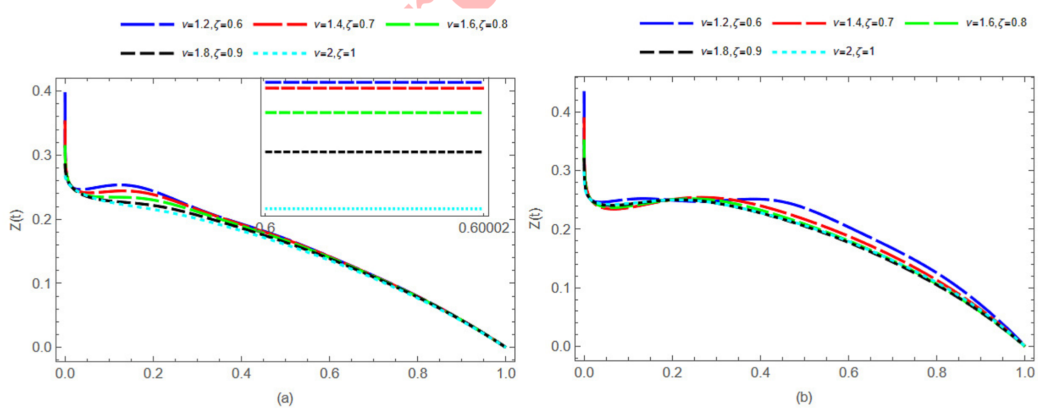

FIGURE 7. Diagrams of $Z(t)$ for $(a): H^2 = 0.5; (b): H^2 = 1$; with $\alpha = 4, \lambda = \frac{2}{50}, n = 9$ and $Activation(t) = \sinh(t)$.

- **Fractional jump-diffusion models:** Integrating fractional jump-diffusion mechanisms to capture sudden flow fluctuations.
- **Regime-switching dynamics:** Extending the methodology to handle regime-dependent systems.

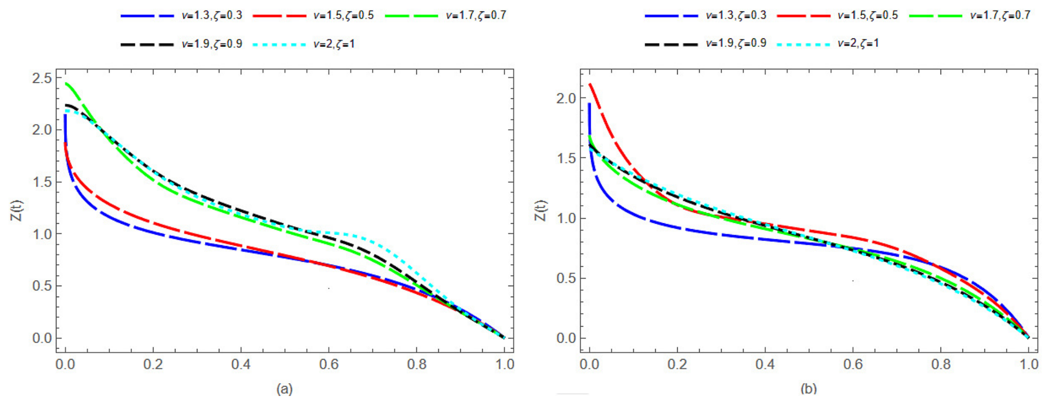

Figure 8. Diagrams of $Z(t)$ for (a) : $H^2 = 5; (b)$: $H^2 = 10$; with $\alpha = 0.5, \lambda = \frac{2}{50}, n = 9$ and $Activation(t) = \sinh(t)$.

- **Rigorous convergence analysis:** Strengthening the theoretical convergence proofs of our ML-augmented MLS approach by utilizing advanced stability analysis techniques for stochastic systems.

Author Contributions. P. R.: Conceptualization, Data curation, Investigation, Software, Writing -original draft.
Z. Kh.M.: Conceptualization, Validation, Writing -review and editing.
E. A.: Conceptualization, Validation, Writing -review and editing.

Data availability statement. Data will be made available on reasonable request.

Funding. The authors received no financial support for the research, authorship, and publication of this paper.

Declaration of Competing Interest. The authors declare that they have no known competing financial interests or personal relationships that could have appeared to influence the work reported in this paper.

Conflict of interest. The authors declare no competing interests.

Acknowledgements

We express our sincere thanks to the anonymous referees for their valuable suggestions that improved the final manuscript.

References

[1] D. Ahmadian, L. V. Ballestra, and N. Karimi, *An extremely efficient numerical method for pricing options in the Black-Scholes model with jumps* , Math. Methods Appl. Sci., *44*(2) (2021), 1843-62.

[2] E. Aourir, N. Izem, and H. L. Dastjerdi, *Numerical solution of third-kind Volterra integral equations with proportional delays based on moving least squares collocation method* , Int. J. Comput. Math., *101* (4) (2024), 447-64.

[3] E. Aourir, and H. L. Dastjerdi, *On the numerical treatments of classes of third-kind auto-convolution VIEs via moving least squares collocation scheme*, Eng. Comput., *42*(2) (2025) 749-79.

[4] M. G. Armentano, and R. G. Durn, *Error estimates for moving least square approximations* , Appl. Numer. Math., *37* (3) (2001), 397–416.

[5] P. Assari, and M. Dehghan, *A meshless local Galerkin method for solving Volterra integral equations deduced from nonlinear fractional differential equations using the moving least squares technique* , Appl. Numer. Math., *143* (2019), 276-99.

[6] M. Driouich, K. Gueraoui, M. Sammouda, Y. M. Haddad, and I. Aberdane,*The effect of electric field on the flow of a compressible ionized fluid in a cylindrical tube*, Adv. Stud. Theor. Phys., *6*(13-16) (2012), 687–96.

[7] K. Edamura, and Y. Otsubo, *A continuous Inkjet device on the basis of electrohydrodynamic mechanism* , J. Imaging. Sci. Technol., *48*(2) (2004) 148–52.

[8] S. Effati, and M. Pakdaman, *Artificial neural network approach for solving fuzzy differential equations*, Inf. Sci. (NY), *180*(8) (2010), 1434–1457.

[9] A. C. Eringen, and G. A. Maugin, *Electrodynamics of continua*, Springer-Verlag, 1990.

[10] O. Farkhondeh Rouz, and D. Ahmadian, *Stability of two classes of improved backward Euler methods for stochastic delay differential equations of neutral type*, Comput. Methods Differ. Equ., *5*(3) (2017), 201-13.

[11] R. H. Gavabari, M. Abbasi, D. D. Ganji, I. Rahimipetroudi, and A. Bozorgi, *Application of Galerkin and collocation method to the electrohydrodyamic flow in a circular cylindrical conduit*, J. Braz. Soc. Mech. Sci. Eng., *38*(8) (2016), 2327–32.

[12] S. E. Ghasemi, M. Hatami, G. R. M. Ahangar, and D. D. Ganji, *Electrohydrodynamic flow analysis in a circular cylindrical conduit using least square method*, J. Electrostat., *72*(1) (2014), 47–52.

[13] N. G. Green, A. Ramos, A. Gonzalez, H. Morgan, and A. Castellanos, *Fluid flow induced by non-uniform AC electric fields in electrolytes on microelectrodes III: Observation of streamlines and numerical simulation* , Phys. Rev. E., *66*(2) (2002), 026305.

[14] J. Han, A. Jentzen, and E. Weinan, *Solving high-dimensional partial differential equations using deep learning* , Proc. Natl. Acad. Sci., *115*(34) (2018), 8505–8510.

[15] Y. Kumar, S. Singh, N. Srivastava, and A. Singh, V. Kumar Singh, *Wavelet approximation scheme for distributed order fractional differential equations*, Comput. Math. Appl., *80*(8) (2020), 1985–2017.

[16] H. Kumar, N. Yadav, A. K. Nagar, *Numerical solution of generalized Burger- Huxley & Huxley's equation using deep Galerkin neural network method* , Eng. Appl. Artif. Intell., *115* (2022), 105289.

[17] H. D. Mazraeh, and K. Parand, *A three-stage framework combining neural networks and Monte Carlo tree search for approximating analytical solutions to the Thomas-Fermi equation* , J. Comput. Sci., *87* (2025), 102582.

[18] J. R. Melcher, *Continuum electromechanics*, MIT Press; 1981.

[19] D. Mirzaei, *Analysis of moving least squares approximation revisited* , J. Comput. Appl. Math., *282* (2015), 237–250.

[20] F. Mirzaee, E. Solhi, and S. Naserifar, *Approximate solution of stochastic Volterra integro-differential equations by using moving least squares scheme and spectral collocation method*, Appl. Math. Comput., *410* (2021), 126447.

[21] S. Mosayebidorcheh, *Taylor series solution of the electrohydrodynamic flow equation*, JMET *1*(2) (2013), 40–5.

[22] H. T. Ngo, T. N. Vo, and M. Razzaghi, *An effective method for solving nonlinear fractional differential equations*, Eng. Comput., *38*(Suppl 1) (2022), 207-18.

[23] P. Rahimkhani, *Deep Neural Network for Solving Stochastic Biological Systems*, Iran. J. Sci., *48*(3) (2024), 687–696.

[24] P. Rahimkhani, *Numerical solution of nonlinear stochastic differential equations with fractional Brownian motion using fractional-order Genocchi deep neural networks*, Commun. Nonlinear Sci. Numer. Simul., *126* (2023), 107466.

[25] P. Rahimkhani, and M. H. Heydari, *Fractional shifted Morgan–Voyce neural networks for solving fractal-fractional pantograph differential equations*, Chaos, Solitons and Fractals *175* (2023), 114070.

[26] P. Rahimkhani, and Y. Ordokhani, *Approximate solution of nonlinear fractional integro-differential equations using fractional alternative Legendre functions*, J. Comput. Appl. Math., *365* (2020), 112365.

[27] P. Rahimkhani, and Y. Ordokhani, *Numerical solution a class of 2D fractional optimal control problems by using 2DMüntz-Legendre wavelets*, Optim. Control Appl. Meth., *39*(6) (2018), 1916–1934.

[28] P. Rahimkhani, Y. Ordokhani, and E. Babolian, *Fractional-order Bernoulli wavelets and their applications*, Appl. Math. Model., *40*(17-18) (2016), 8087–8107.

[29] P. Rahimkhani, Y. Ordokhani, and E. Babolian, *Numerical solution of fractional pantograph differential equations by using generalized fractional-order Bernoulli wavelet*, J. Comput. Appl. Math., *309* (2017), 493-510.

[30] S. Rashidi, J. A. Esfahni, and M. Maskaniyan, *Applications of magnetohydrodynamics in biological systems- a review on the numerical studies*, J. Magn. Magn. Mater., *439* (2017), 358–72.

[31] A. Rayal, and S. R. Verma, *Numerical analysis of pantograph differential equation of the stretched type associated with fractal-fractional derivatives via fractional order Legendre wavelets*, Chaos Solitons Fractals, *139* (2020), 110076.

[32] P. Roul, H. Madduri, and K. Kassner, *A new iterative algorithm for a strongly nonlinear singular boundary value problem*, J. Comput. Appl. Math., *351* (2019), 167–78.

[33] M. N. Sahlan, and H. Afshari, *Lucas polynomials based spectral methods for solving the fractional order electrohydrodynamics flow model*, Commun. Nonlinear Sci. Numer. Simul., *107* (2022), 106108.

[34] A. Safdari-Vaighani, D. Ahmadian, and R. Javid-Jahromi, *An approximation scheme for option pricing under two-state continuous CAPM*, Comput. Econ., *57*(4) (2021), 1373-85.

[35] H. M. Srivastava, and M. Izadi, *Generalized shifted airfoil polynomials of the second kind to solve a class of singular electrohydrodynamic fluid model of fractional order*, Fractal Fract., *7*(1) (2023), 94.

[36] E. Tanojo, *Derivation of moving least-squares approximation shape functions and its derivatives using the exponential weight function*, Civil Engin. Dimen., *9*(1) (2007), 19–24.

[37] S. Thirumalai, and R. Seshadri, *Spectral solutions of fractional differential equation modelling electrohydrodynamics flow in a cylindrical conduit*, Commun. Nonlinear Sci. Numer. Simul., *79* (2019), 104931.

[38] H. Wendland, *Scattered data approximation*, Cambridge University Press, Cambridge. 2005.

[39] C. Xiaopeng, C. Jiusheng, and Y. Xiezhen, *Advances and applications of electrohydrodynamics*, Chin. Sci. Bull., *48*(11) (2003), 1055–63.

[40] H. Zhang, Y. Xu, Q. Liu, and Y. Li, *Deep learning framework for solving Fokker-Planck equations with low-rank separation representation*, Eng. Appl. Artif. Intell., *121* (2023), 106036.

[41] N. Zobeiry, and K. D. Humfeld, *A physics-informed machine learning approach for solving heat transfer equation in advanced manufacturing and engineering applications*, Eng. Appl. Artif. Intell., *101* (2021), 104232.

[42] C. Zuppa, *Error estimates for moving least square approximations*, Bull. Braz. Math. Soc. New. Series, *34* (2) (2003) 231–249.